

Characteristics of space-time energy spectra in turbulent channel flows

Ting Wu,^{1,2} Chenhui Geng,^{1,2} Yichen Yao,³ Chunxiao Xu,³ and Guowei He^{1,2,*}

¹*The State Key Laboratory of Nonlinear Mechanics, Institute of Mechanics, Chinese Academy of Sciences, Beijing 100190, China*

²*School of Engineering Sciences, University of Chinese Academy of Sciences, Beijing 100049, China*

³*Department of Engineering Mechanics, Tsinghua University, Beijing 100084, China*

(Received 18 January 2017; published 31 August 2017)

An energy spectrum is preliminarily characterized by its mean and standard deviation. In this study, we derive exact expressions for the means and bandwidths of space-time energy spectra at fixed frequencies. The mean wave numbers are used to determine the phase velocities that bridge from temporal spectra to space-time spectra. The bandwidths are used to measure the well-known spectral broadening. We show that phase velocities alone are insufficient to determine the bandwidths of energy spectra. As a result, the cross-spectral method predicts narrower bandwidths of energy spectra. Therefore, in addition to phase velocities, amplitudes are used to rescale the space-time energy spectra, leading to the correct bandwidths. Existing data from direct numerical simulations of turbulent channel flows validate the rescaling approach.

DOI: [10.1103/PhysRevFluids.2.084609](https://doi.org/10.1103/PhysRevFluids.2.084609)

I. INTRODUCTION

Space-time energy spectra of velocity fluctuations describe the energy distribution in turbulent flows over length and time scales. These spectra are particularly useful in studies of multi-scale coupling in space and time [1,2]. However, obtaining full space-time energy spectra from experimental measurements remains challenging [3] because only a subset of the spatial and temporal signals of the velocity fluctuations is experimentally available.

Taylor's frozen-flow hypothesis [4] was proposed to determine spatial energy spectra from temporal signals in hot-wire experiments. According to Taylor's hypothesis, turbulent velocity fluctuations propagate downstream at the convection velocity and remain unchanged during the propagation process. The convection velocity is usually defined by space-time correlations or space-time energy spectra [5–7], in which the dependences of the convection velocity on the wave number and frequency have been thoroughly investigated [8,9]. In Taylor's frozen-flow hypothesis, the widths of the energy spectra vanish, which implies that the eddies of individual frequencies have a single wave number and *vice versa*. However, the widths of space-time energy spectra in turbulent flows do not vanish due to random sweeping [10,11] and shear distortion [12,13], which lead to spectral broadening [14]. The issue of spectral spreading is important for reconstructing space-time energy spectra.

Wilczek and Narita [15] derive an advection model based on the Kraichnan-Tennekes random sweeping hypothesis [10,11] with additional mean flows, which predicts the space-time spectra from the energy spectra in the wave-vector domain. This model clarifies that the mean velocity leads to a Doppler shift of the frequencies, whereas the sweeping velocity causes a Doppler broadening. Wilczek *et al.* [16,17] show the applicability of the random sweeping model with a mean flow in the logarithmic layer of turbulent channel flow.

The cross-spectral approach [18,19] was developed experimentally to investigate frequency-dependent convection velocities from two-point cross correlations, such as those obtained from laser Doppler anemometry (LDA) and particle image velocimetry (PIV) measurements; however,

*Corresponding author: hgw@lnm.imech.ac.cn

these studies neglect the variation in the phase velocities. Buxton *et al.* [20] show that the phase velocities obtained from the cross-spectral approach are spread over a certain range. Following up on this work, de Kat and Ganapathisubramani [21] apply the cross-spectral approach to generate a transfer function that can map the temporal energy spectra to space-time spectra. This method uses the phases of the velocity modes to construct the maps from temporal spectra to space-time spectra and yields the correct shapes of the space-time spectra. However, whether the phase velocities (or phase differences) alone can be used to correctly determine the characteristics of the space-time energy spectra remains unknown.

A space-time energy spectrum can be preliminarily characterized by its first-order and second-order moments. For example, given a frequency, the first-order moment of an energy spectrum indicates the energy-weighted average of the wave numbers. The mean wave number can be used to calculate the phase velocity and thus determines the convection velocity in Taylor's frozen-flow hypothesis. The second-order moments of space-time energy spectra give the spectral bandwidths and can be used to validate Taylor's frozen-flow hypothesis. It is noted that Taylor's hypothesis with a constant convection velocity leads to a vanishing bandwidth [22]. Del Álamo and Jiménez [8] propose that the convection velocities are dependent on both streamwise and spanwise wavelengths, which generate non-vanishing bandwidths. In this paper, we study the extent to which the phases of the velocity modes alone can correctly determine the mean wave numbers and the bandwidths of space-time energy spectra. The bandwidths will be used to rescale the maps in the cross-spectral approach to reconstruct the space-time energy spectra.

This paper is organized as follows. In Sec. II, we derive exact expressions for the mean wave numbers and bandwidths. The results are used to evaluate the reconstruction approaches for space-time energy spectra, such as Taylor's frozen-flow hypothesis. In Sec. III, we investigate the mean wave numbers and spectral bandwidths in turbulent channel flows, using their exact expressions. In Sec. IV, the bandwidths are used to rescale the space-time energy spectra obtained from the cross-spectral approach, which are consistent with direct numerical simulation (DNS) results. Finally, we present the conclusions and future work in Sec. V.

II. THE EXACT EXPRESSIONS FOR THE MEAN WAVE NUMBERS AND SPECTRAL BANDWIDTHS

The mean wave numbers and bandwidths for space-time energy spectra are most simply examined in the one-dimensional case. Therefore, we consider a one-dimensional velocity field $u(x, t)$ in this section. The results will be easily extended to three-dimensional cases in the next section. If the space-time Fourier modes of the velocity $u(x, t)$ are denoted as $\hat{u}(k_x, \omega)$, the space-time energy spectrum is written as

$$\Phi(k_x, \omega) = \frac{\langle \hat{u}^*(k_x, \omega) \hat{u}(k_x, \omega) \rangle}{\Delta k_x \Delta \omega}, \quad (1)$$

where $\Delta k_x = 2\pi/L_x$, $\Delta \omega = 2\pi/T$, L_x is the domain size, T is the largest characteristic timescale, and $\langle (\cdot) \rangle$ is the ensemble average. The space-time energy spectrum $\Phi(k_x, \omega)$ is a two-dimensional surface with respect to the wave number k_x and the frequency ω . It can also be regarded as a family of curves $\{\Phi(k_x, \omega) : \omega\}$ in which each curve is the spatial energy spectrum at a given frequency ω . For a fixed frequency ω , we define the mean wave number and the bandwidth for the spatial energy spectrum $\Phi(k_x, \omega)$ as

$$k_{xc}(\omega) = \frac{\int k_x \Phi(k_x, \omega) dk_x}{\Phi_t(\omega)}, \quad (2)$$

$$B(\omega) = \frac{\int (k_x - k_{xc}(\omega))^2 \Phi(k_x, \omega) dk_x}{\Phi_t(\omega)}, \quad (3)$$

where $\Phi_t(\omega)$ is the temporal energy spectrum. The mean wave number $k_{xc}(\omega)$ is the energy-weighted average of the wave numbers for the frequency ω , from which the frequency-dependent convection velocities are estimated as $U_c(\omega) = \omega/k_{xc}(\omega)$ [8,9,18,19]. $B(\omega)$ is the standard variance of $\Phi(k_x, \omega)$, which gives the extent of the wave numbers to the mean wave number $k_{xc}(\omega)$.

In experiments, the velocity field $u(x, t)$ is often measured at a fixed location x , and the temporal Fourier modes $\hat{u}(x, \omega)$ are obtained through Fourier transformations. To understand the contributions of the amplitudes and phases to the mean wave numbers and spectral bandwidths, we derive their exact expressions as functions of the amplitudes $|\hat{u}(x, \omega)|$ and phase $\theta(x, \omega)$, where

$$\hat{u}(x, \omega) = |\hat{u}(x, \omega)| \exp[i\theta(x, \omega)]. \quad (4)$$

To do this, we introduce the mode correlations at two locations x and $x + r$,

$$R(r, \omega) = \frac{\langle \hat{u}^*(x, \omega) \hat{u}(x + r, \omega) \rangle}{\langle \hat{u}^*(x, \omega) \hat{u}(x, \omega) \rangle}, \quad (5)$$

which are related to the space-time energy spectra by

$$R(r, \omega) = \frac{\int \Phi(k_x, \omega) \exp(ik_x r) dk_x}{\Phi_t(\omega)}. \quad (6)$$

Taking the first and second derivatives of Eq. (6) with respect to r at $r = 0$, we obtain

$$\left. \frac{\partial R(r, \omega)}{\partial r} \right|_{r=0} = ik_{xc}(\omega), \quad (7)$$

and

$$\left. \frac{\partial^2 R(r, \omega)}{\partial r^2} \right|_{r=0} = -B(\omega) - k_{xc}^2(\omega). \quad (8)$$

The terms on the left-hand sides of Eqs. (7) and (8) can be evaluated using Eqs. (5) and (4), which are given by

$$\left. \frac{\partial R(r, \omega)}{\partial r} \right|_{r=0} = \frac{\langle \hat{u}^* \partial_x \hat{u} \rangle}{\langle |\hat{u}|^2 \rangle} = i \frac{\langle |\hat{u}|^2 \partial_x \theta \rangle}{\langle |\hat{u}|^2 \rangle} \quad (9)$$

and

$$\left. \frac{\partial^2 R(r, \omega)}{\partial r^2} \right|_{r=0} = \frac{\langle \hat{u}^* \partial_{xx}^2 \hat{u} \rangle}{\langle |\hat{u}|^2 \rangle} = -\frac{\langle |\hat{u}|^2 (\partial_x \theta)^2 \rangle}{\langle |\hat{u}|^2 \rangle} - \frac{\langle (\partial_x |\hat{u}|)^2 \rangle}{\langle |\hat{u}|^2 \rangle}, \quad (10)$$

where integration by parts and the homogeneity assumption are used. By substituting Eqs. (9) and (10) into Eqs. (7) and (8), we obtain the exact expressions for the mean wave numbers and the spectral bandwidths

$$k_{xc}(\omega) = \frac{\langle |\hat{u}|^2 \partial_x \theta \rangle}{\langle |\hat{u}|^2 \rangle}, \quad (11)$$

$$B(\omega) = \underbrace{\frac{\langle |\hat{u}|^2 (\partial_x \theta - k_{xc})^2 \rangle}{\langle |\hat{u}|^2 \rangle}}_{\text{Term I}} + \underbrace{\frac{\langle (\partial_x |\hat{u}|)^2 \rangle}{\langle |\hat{u}|^2 \rangle}}_{\text{Term II}}. \quad (12)$$

The phase derivative $\partial_x \theta$ can be interpreted as a local wave number. Therefore, Eq. (11) implies that the mean wave number $k_{xc}(\omega)$ is the energy-weighted average of the local wave numbers for a given frequency ω . Equation (12) implies that the spectral bandwidth is determined by two terms: ‘‘Term I’’ is associated with the phase derivative, and ‘‘Term II’’ is associated with the amplitude derivative. In other words, both the phase and the amplitude contribute to the spectral bandwidths.

If $u(x, t)$ satisfies Taylor's frozen-flow hypothesis, the velocity at a future time $t + \tau$ is

$$u(x, t + \tau) = u(x - U\tau, t), \quad (13)$$

where U is a constant convection velocity. Therefore, its temporal Fourier mode $\hat{u}(x, \omega)$ can be expressed as

$$\hat{u}(x, \omega) = \hat{u}(0, \omega) \exp\left(i\frac{\omega x}{U}\right), \quad (14)$$

which leads to $\partial_x \theta = \omega/U$ and $\partial_x |\hat{u}| = 0$. According to Eqs. (11) and (12), the mean wave number and bandwidth in Taylor's hypothesis are given by

$$k_{xc}^{TA}(\omega) = \omega/U \quad (15)$$

and

$$B^{TA}(\omega) = 0, \quad (16)$$

respectively, where the superscript "TA" denotes the results from Taylor's hypothesis. Therefore, the spectral bandwidths in Taylor's frozen-flow hypothesis are zero. However, if the convection velocity U exhibits spatial fluctuations and thus $\partial_x \theta - k_{xc} \neq 0$, the bandwidths may not be zero [$B(\omega) \neq 0$], which implies "spectral broadening" [14]. McKeon and Sharma suggest that Taylor's hypothesis would be better validated in terms of the bandwidths of the space-time energy spectra [22].

If $u(x, t)$ satisfies the random-sweeping hypothesis [10, 13] in one dimension, its temporal Fourier mode can be written as

$$\hat{u}(x, \omega) = \hat{u}(0, \omega) \exp\left(i\frac{\omega x}{v}\right), \quad (17)$$

where $\partial_x \theta = \omega/v$, $\partial_x |\hat{u}| = 0$, and the random velocity v is constant in space and time and satisfies a symmetric probability distribution with a mean of zero. Substituting Eq. (17) into Eqs. (11) and (12) yields

$$k_{xc}^{SW}(\omega) = 0, \quad (18)$$

$$B^{SW}(\omega) = \left\langle \left(\frac{\omega}{v}\right)^2 \right\rangle > 0, \quad (19)$$

where the superscript "SW" denotes the results from the random-sweeping hypothesis. The results are consistent with those calculated from definitions (2) and (3). Therefore, the spectral bandwidths in the random-sweeping hypothesis are non-zero.

III. THE MEAN WAVE NUMBERS AND SPECTRAL BANDWIDTHS IN TURBULENT CHANNEL FLOWS

In this section, we use the exact expressions in Eqs. (11) and (12) to investigate the mean wave numbers and spectral bandwidths in turbulent channel flows. The interesting finding is that both the amplitudes and phases make significant contributions to the spectral bandwidths; the phases alone are insufficient to determine the spectral bandwidths.

In this study, we use data from DNS of turbulent channel flows at $\text{Re}_\tau \equiv u_\tau h/\nu = 550$ [23–25], where u_τ is the friction velocity, h is the channel half-width, and ν is the kinematic viscosity. The bulk Reynolds number is $\text{Re} \equiv U_b h/\nu = 10000$, where U_b is the bulk velocity. A pseudo-spectral method is used to numerically solve the Navier-Stokes equations [26]. Periodic boundary conditions are employed in the homogeneous streamwise and spanwise directions, and no-slip boundary conditions are applied in the wall-normal direction. The dimensions of the computational domain are $8\pi h \times 2h \times 3\pi h$ in the streamwise (x), wall-normal (y), and spanwise (z) directions, respectively, and the domain contains $1536 \times 256 \times 1152$ grid points. The time step is taken as

$\Delta t = 1.25 \times 10^{-3} h/U_b$ ($\Delta t^+ \approx 0.037$, and “+” indicates normalization with the viscous scales). The instantaneous velocity fields are stored every eight time steps during a period of $20.48h/U_b$ in the statistically stationary state. We ran two DNS cases of turbulent channel flows at $Re_\tau = 180$ and 550 . The results at $Re_\tau = 180$ are consistent with those of Moser *et al.* [27], which are not used in the present paper. The results at $Re_\tau = 550$ are consistent with those of Del Álamo and Jiménez [28] and will be used in the present paper.

In turbulent channel flows, the streamwise velocity fluctuations $u(x, y, z; t)$ are homogeneous in the spanwise direction but inhomogeneous in the wall-normal direction. To clarify this, we explicitly express the dependencies of the velocities and their related physical quantities on the wall-normal locations y . For example, the spatial, temporal and space-time Fourier modes of $u(x, y, z; t)$ are written as $\hat{u}(k_x, y, z; t)$, $\hat{u}(x, y, z; \omega)$, and $\hat{u}(k_x, y, z; \omega)$, respectively. In cases with no confusion, these modes can be abbreviated as $\hat{u}(k_x, t; y)$, $\hat{u}(x, \omega; y)$, and $\hat{u}(k_x, \omega; y)$, respectively. We calculate the temporal Fourier modes from the DNS data using the Hanning window as follows [29,30]:

$$\hat{u}(x, \omega; y) = \frac{1}{\sqrt{T \int_0^T w(t)^2 dt}} \int_0^T w(t) u(x, t; y) \exp(i\omega t) dt, \quad (20)$$

where w is the Hanning window. The temporal length T of the window is taken as $T = 5.12h/U_b$. Furthermore, we calculate the streamwise space-time Fourier modes

$$\hat{u}(k_x, \omega; y) = \frac{1}{L_x} \int_0^{L_x} \hat{u}(x, \omega; y) \exp(-ik_x x) dx. \quad (21)$$

Using those definitions, the space-time energy spectrum $\Phi(k_x, \omega; y)$ can be calculated from Eq. (1). In particular, the spatial energy spectrum $\Phi_s(k_x; y)$ and the temporal energy spectrum $\Phi_t(\omega; y)$ can be obtained by integrating $\Phi(k_x, \omega; y)$ with respect to the wave number k_x and the frequency ω , respectively:

$$\Phi_s(k_x; y) = \sum_{\omega} \Phi(k_x, \omega; y) \Delta\omega, \quad \Phi_t(\omega; y) = \sum_{k_x} \Phi(k_x, \omega; y) \Delta k_x. \quad (22)$$

Finally, the mean wave number $k_{xc}(\omega; y)$ and the bandwidth $B(\omega; y)$ of $\Phi(k_x, \omega; y)$ can be calculated from Eqs. (2) and (3), respectively.

Figure 1(a) compares the space-time energy spectrum at $y^+ = 92$ obtained from the DNS of turbulent channel flows at $Re_\tau = 550$ with the spectrum from Taylor’s hypothesis, where $\Phi^{TA}(k_x, \omega) = \Phi_t(\omega) \delta(k_x - \omega/U)$, and U is the convection velocity. The former is a two-dimensional surface, and the latter is a single curve. Consequently, the spectral bandwidth in Taylor’s hypothesis is zero. However, it is not zero in the DNS. The true values of the bandwidths are presented in Fig. 3. For further comparison, Fig. 1(b) shows sketches of the spatial energy spectra from Taylor’s hypothesis and the DNS at a given frequency. The results from Taylor’s frozen-flow hypothesis are concentrated at a single wave number, and those from the DNS are distributed over a range of wave numbers. Figure 2 compares the mean wave numbers from the exact expression (11) and the DNS, which are in good agreement.

Figure 3 plots the bandwidths of the space-time energy spectra at $y^+ = 92$ obtained from the DNS and the exact expression [Eq. (12)] for the spectral bandwidths. Using the existing DNS database of turbulent channel flows, we calculate the space-time energy spectra and estimate their bandwidths. We also calculate the temporal modes of the velocity fluctuations and use the exact expression for the spectral bandwidths [Eq. (12)] to determine the bandwidths. The results are in agreement. An important finding is that the amplitude contribution associated with “Term II” is large compared to the phase contribution associated with “Term I”. Therefore, the amplitude contribution to the bandwidths in turbulent channel flows cannot be ignored.

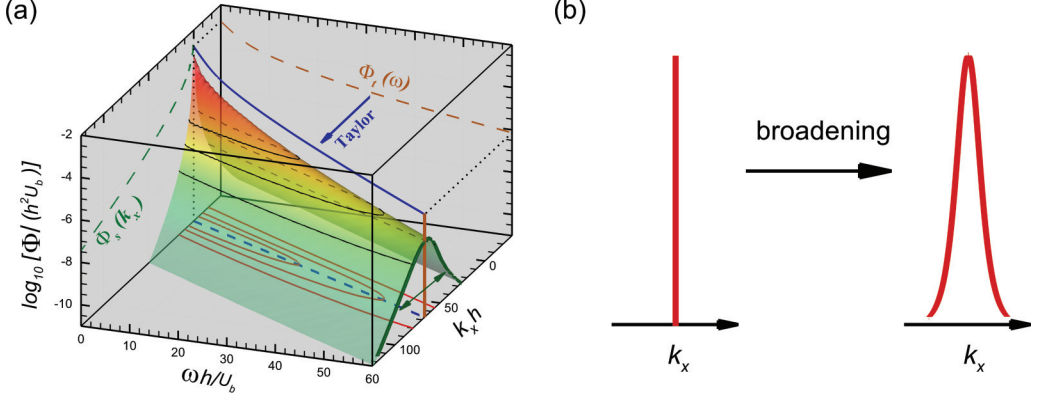


FIG. 1. (a) Space-time energy spectra of the streamwise velocity at $y^+ = 92$ in turbulent channel flows at $Re_\tau = 550$. The colored surface shows the energy spectra Φ from the DNS, and the blue solid line indicates the energy spectra obtained using Taylor's hypothesis. The spatial energy spectra $\Phi_s(k_x)$ (green dashed line) and temporal energy spectra $\Phi_t(\omega)$ (brown dashed line) are also plotted for comparison. The spectrum contours (red solid lines) are aligned in the preferential direction (blue dashed line) $\omega = k_x U$ indicated by Taylor's hypothesis. The transverse curve (green solid line) indicates the spatial energy spectrum at a fixed frequency ($\omega h / U_b = 60$) from the DNS, and the straight line (brown solid line) indicates the spectrum from Taylor's hypothesis. (b) Sketch of the spatial energy spectra at a fixed frequency obtained from Taylor's hypothesis (left figure) and the DNS (right figure), which illustrates "spectral broadening".

IV. SPACE-TIME ENERGY SPECTRA FROM THE CROSS-SPECTRAL METHOD

de Kat and Ganapathisubramani [21] propose the cross-spectral method (hereafter referred to as the CS method) to reconstruct space-time energy spectra. This method uses two-point measurements, in which time series of the velocity fluctuations at pair-points are recorded. The method can be described as follows:

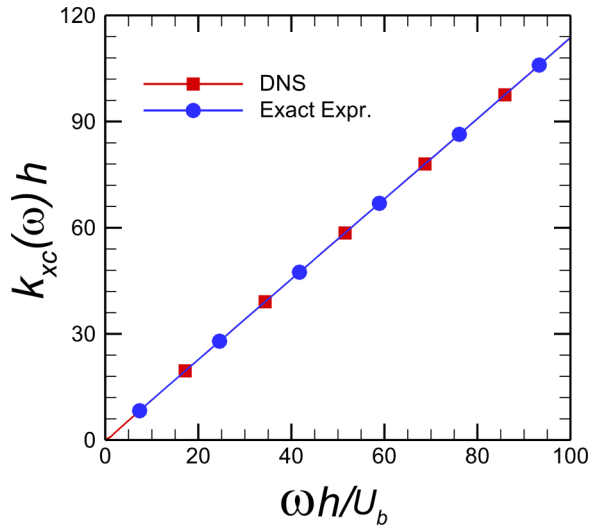


FIG. 2. Mean wave numbers of the space-time energy spectra at $y^+ = 92$ obtained from the DNS and the exact expression in Eq. (11).

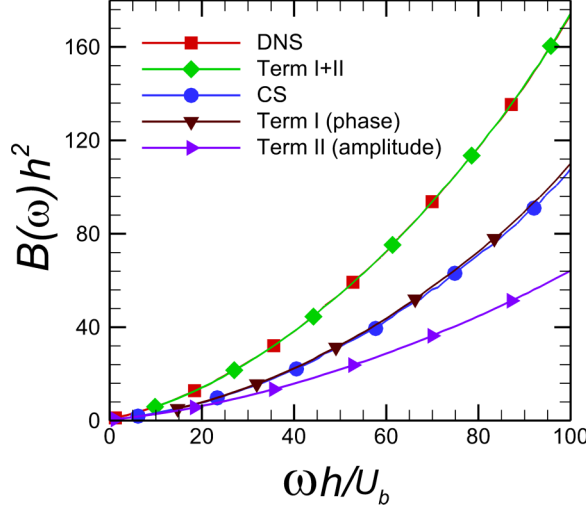


FIG. 3. Bandwidths of the space-time energy spectra at $y^+ = 92$ obtained from the DNS, the exact expression [Term I+II in Eq. (12)] and the cross-spectral method. The phase contribution (Term I) and the amplitude contribution (Term II) are also plotted.

(1) The cross-spectrum Ψ is calculated in terms of

$$\Psi(x, \omega; \Delta x; y) = \hat{u}^*(x, \omega; y) \hat{u}(x + \Delta x, \omega; y) = |\Psi| \exp(i\Delta\theta), \quad (23)$$

where $|\Psi|$ is the cross-spectral energy, and $\Delta\theta$ is the phase difference between $\hat{u}(x, \omega; y)$ and $\hat{u}(x + \Delta x, \omega; y)$. The phase difference $\Delta\theta$ can be simply obtained from the cross-spectra, $\Delta\theta = \arctan[\text{Im}(\Psi)/\text{Re}(\Psi)]$, and used to estimate the local wave number k_x^{CS} for a given frequency ω

$$k_x^{CS}(x, \omega; \Delta x; y) = \frac{\Delta\theta}{\Delta x}. \quad (24)$$

(2) The transfer function is determined from the cross-spectrum

$$G^{CS}(k_x, \omega; \Delta x; y) = \frac{\sum_{k_x^{CS} \in \text{Bin}(k_x)} |\Psi(x, \omega; \Delta x; y)|}{\Delta k_x \sum_x |\Psi(x, \omega; \Delta x; y)|}, \quad (25)$$

where $\text{Bin}(k_x) \equiv [k_x - \Delta k_x/2, k_x + \Delta k_x/2]$ is an interval centered at the wave number k_x with a width Δk_x . The summation in the numerator is taken for the locations x such that the local wave number $k_x^{CS}(x, \omega; \Delta x; y)$ belongs to $\text{Bin}(k_x)$, and the summation in the denominator is taken for the samples at all locations x . Therefore, the transfer function is the normalized space-time energy spectrum that satisfies $\int G^{CS}(k_x, \omega; \Delta x; y) dk_x = 1$. The accuracy of the transfer functions is dependent on the sample number of the pair of points and the correct choice of bins.

(3) The space-time energy spectrum is reconstructed from the transfer function $G^{CS}(k_x, \omega; \Delta x; y)$ and the temporal energy spectrum $\Phi_t(\omega; y)$

$$\Phi^{CS}(k_x, \omega; \Delta x; y) = \Phi_t(\omega; y) G^{CS}(k_x, \omega; \Delta x; y), \quad (26)$$

where $\int \Phi^{CS}(k_x, \omega; \Delta x; y) dk_x = \Phi_t(\omega; y)$.

In the CS method, the sample of the phase differences at the pair-points is used to determine all possible wave numbers that correspond to a fixed frequency. Therefore, this method can account for the spectral broadening. However, in Taylor's frozen-flow hypothesis, only one wave number is obtained for this fixed frequency through a constant convection velocity. As a result, it excludes

the spectral broadening. In fact, the convection velocity in Taylor's hypothesis is the average of the phase velocities in the CS method.

In the limit of $\Delta x \rightarrow 0$, the cross-spectral energy is

$$\Psi(x, \omega; y) \equiv \Psi(x, \omega; \Delta x \rightarrow 0; y) = |\hat{u}(x, \omega; y)|^2, \quad (27)$$

and the local wave number is

$$k_x^{CS}(x, \omega; y) \equiv k_x^{CS}(x, \omega; \Delta x \rightarrow 0; y) = \partial_x \theta. \quad (28)$$

Therefore, using the definition of the mean wave number k_{xc} , the mean wave numbers in the CS method can be expressed as

$$k_{xc}^{CS}(\omega; y) = \frac{\langle |\hat{u}|^2 k_x^{CS} \rangle}{\langle |\hat{u}|^2 \rangle} = \frac{\langle |\hat{u}|^2 \partial_x \theta \rangle}{\langle |\hat{u}|^2 \rangle}. \quad (29)$$

Hence, the CS method can predict the mean wave numbers. We now calculate the bandwidth of the space-time energy spectrum in the CS method using the local wave number k_x^{CS} and the mean wave number k_{xc}^{CS}

$$B^{CS}(\omega; y) = \frac{\langle |\hat{u}|^2 (k_x^{CS} - k_{xc}^{CS})^2 \rangle}{\langle |\hat{u}|^2 \rangle} = \frac{\langle |\hat{u}|^2 (\partial_x \theta - k_{xc})^2 \rangle}{\langle |\hat{u}|^2 \rangle}. \quad (30)$$

Consequently, the CS method correctly predicts "Term I", which is associated with the phases in Eq. (12). It is a good approximation for the spectral bandwidths for the frozen amplitudes $\partial_x |\hat{u}| = 0$.

The bandwidths $B^{CS}(\omega; y)$ of the space-time energy spectra obtained from the CS method are plotted in Fig. 3. They are consistent with the predictions from "Term I" in Eq. (12). However, the bandwidths $B^{CS}(\omega; y)$ are smaller than the DNS results. This implies that the contribution of the amplitude to the bandwidths in turbulent channel flows cannot be ignored.

The CS method utilizes phase derivatives but does not account for amplitude derivatives. To account for the amplitude derivatives, we propose a rescaling technique for the transfer function G^{CS} . This technique is described as follows:

(1) We calculate the ratio of $B^{CS}(\omega; y)$ to $B(\omega; y)$

$$\eta(\omega; y) = \frac{B^{CS}(\omega; y)}{B(\omega; y)} = \frac{\langle |\hat{u}|^2 (\partial_x \theta - k_{xc})^2 \rangle}{\langle |\hat{u}|^2 (\partial_x \theta - k_{xc})^2 \rangle + \langle (\partial_x |\hat{u}|)^2 \rangle}, \quad (31)$$

where $B(\omega; y)$ is the true value of the spectral bandwidth, which can be obtained from two-point measurements. It is explicitly dependent on the amplitude derivatives.

(2) A linear transformation is performed on the local wave numbers and the transfer function in the CS method

$$k_x \rightarrow \sqrt{\eta}(k_x - k_{xc}^{CS}) + k_{xc}^{CS}, \quad (32)$$

$$G^{CS} \rightarrow \sqrt{\eta} G^{CS}. \quad (33)$$

As a result, we obtain the rescaled transfer function

$$G^{RS}(k_x, \omega; \Delta x; y) = \sqrt{\eta} G^{CS}(\sqrt{\eta}(k_x - k_{xc}^{CS}) + k_{xc}^{CS}, \omega; \Delta x; y), \quad (34)$$

where the superscript "RS" denotes the results from the rescaling technique. The rescaled transfer functions can be shown to give the exact mean wave numbers and spectral bandwidths. In fact, the rescaled transfer function (34) is used to calculate the space-time energy spectra (26). The results are then substituted into Eqs. (2) and (3), which lead to

$$k_{xc}^{RS}(\omega; y) = k_{xc}^{CS}(\omega; y) = \frac{\langle |\hat{u}|^2 \partial_x \theta \rangle}{\langle |\hat{u}|^2 \rangle} \quad (35)$$

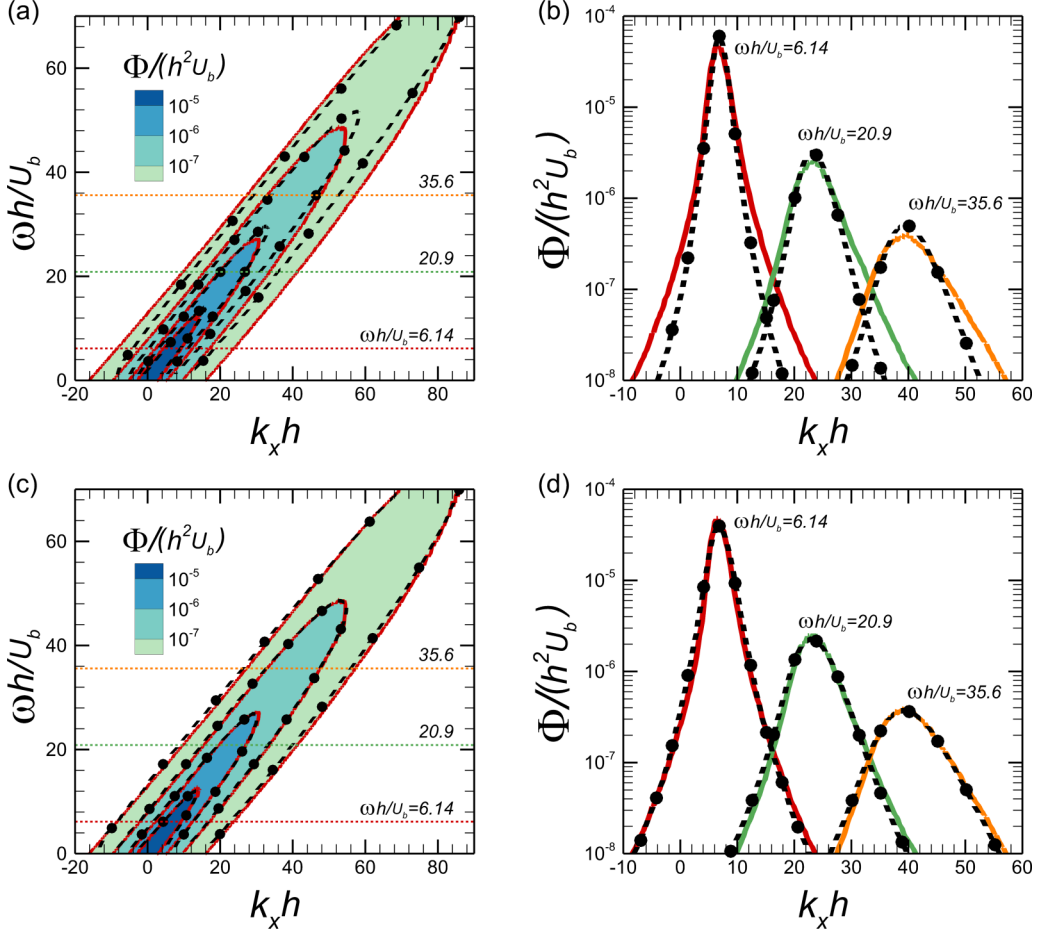


FIG. 4. Comparisons of the space-time energy spectra at $y^+ = 92$ obtained from the DNS and the reconstruction methods. (a) Contours of the space-time energy spectra obtained from the DNS (colored shades) and the cross-spectral method (dashed lines with dots). (b) Spatial energy spectra at three frequencies obtained from the DNS (colored solid lines) and the cross-spectral method (dashed lines with dots). (c) Contours of the space-time energy spectra obtained from the DNS (colored shades) and the rescaling technique (dashed lines with dots). (d) Spatial energy spectra at three frequencies obtained from the DNS (colored solid lines) and the rescaling technique (dashed lines with dots).

and

$$B^{RS}(\omega; y) = \frac{1}{\eta(\omega; y)} B^{CS}(\omega; y) = B(\omega; y) = \frac{\langle |\hat{u}|^2 (\partial_x \theta - k_{xc})^2 \rangle}{\langle |\hat{u}|^2 \rangle} + \frac{\langle (\partial_x |\hat{u}|)^2 \rangle}{\langle |\hat{u}|^2 \rangle}, \quad (36)$$

which are the right-hand terms of Eqs. (11) and (12), respectively. The rescaling technique requires the true values of the spectral bandwidths, including the amplitude derivatives, which can be obtained from two-point measurements. This result suggests the potential extension of the CS method to correctly predict the spectral bandwidths.

The space-time energy spectra at $y^+ = 92$ from the DNS, the CS method and the rescaling approach are compared in Fig. 4. In this study, Δx is taken to be the same as the streamwise mesh size. The unfolding technique [20,21] is used to calculate $\Delta\theta$, where $\Delta\theta$ is unfolded into the range $\omega\Delta x/U_c - \pi < \Delta\theta < \omega\Delta x/U_c + \pi$ and U_c is an estimated convection velocity. For Eq. (25), the

width Δk_x of $\text{Bin}(k_x)$ is taken as $\pi/(300\Delta x)$. In Figs. 4(a) and 4(b), we compare the results from the DNS with those from the CS method. The CS method can map the temporal energy spectra to the space-time energy spectra in terms of the shape. However, their bandwidths are distinctly narrower than the DNS results, because the amplitude derivatives are ignored. The comparisons of the space-time energy spectra from the DNS and the rescaling approach are presented in Figs. 4(c) and 4(d), and they are in good agreement. In fact, the comparisons at $y^+ = 5, 12, 44,$ and 270 , which are not shown due to space limitations, are also in close agreement. Therefore, we find that the CS method can obtain a good estimate of the shape of the space-time energy spectra and that the rescaling approach makes further improvements by including the effect of the amplitude derivative. In summary, it is observed by the use of the DNS data of turbulent channel flows that the results obtained from the rescaling technique are in good agreement with those directly calculated from the numerical channel. The rescaling technique offers a remedy for the CS method. Therefore, a reconstructive method that essentially includes the amplitude contributions needs to be developed.

V. CONCLUSIONS AND FUTURE WORK

This paper uses the mean wave numbers and bandwidths to characterize the space-time energy spectra in turbulent shear flows. We derive exact expressions for the means and bandwidths. The exact expressions show that the bandwidths of the energy spectra are determined by both the amplitudes and phases of the velocity modes. Therefore, the phase velocity alone is not sufficient to determine the bandwidths of the energy spectra in turbulent shear flows.

The expressions for the bandwidths are further used to evaluate the approaches to reconstruct space-time energy spectra. Taylor's frozen-flow hypothesis is shown to lead to vanishing bandwidths and thus cannot be used to reconstruct space-time energy spectra. The cross-spectral method precisely predicts the phase contributions to the bandwidths. However, it does not account for the amplitude contributions, which results in narrower bandwidths. The DNS results demonstrate that the rescaling approach for the cross-spectral method, which uses both the amplitude and phase, can correctly estimate the bandwidths of space-time energy spectra. Therefore, future work will focus on incorporating the amplitude information into the cross-spectral method.

ACKNOWLEDGMENTS

This work was supported by National Natural Science Foundation of China (No. 11302238, No. 11232011, No. 11572331, and No. 11490551). The authors would like to acknowledge the support from the Strategic Priority Research Program (Grant No. XDB22040104) and the Key Research Program of Frontier Sciences of the Chinese Academy of Sciences (Grant No. QYZDJ-SSW-SYS002) and the National Basic Research Program of China (973 Program No. 2013CB834100: Nonlinear science).

-
- [1] G. W. He, G. D. Jin, and Y. Yang, Space-time correlations and dynamic coupling in turbulent flows, *Annu. Rev. Fluid Mech.* **49**, 51 (2016).
 - [2] J. M. Wallace, Space-time correlations in turbulent flow: A review, *Theor. Appl. Mech. Lett.* **4**, 022003 (2014).
 - [3] J. LeHew, M. Guala, and B. J. McKeon, A study of the three-dimensional spectral energy distribution in a zero pressure gradient turbulent boundary layer, *Exp. Fluids* **51**, 997 (2011).
 - [4] G. I. Taylor, The spectrum of turbulence, *Proc. R. Soc. Lond. A* **164**, 476 (1938).
 - [5] W. W. Willmarth and C. E. Wooldridge, Measurements of the fluctuating pressure at the wall beneath a thick turbulent boundary layer, *J. Fluid Mech.* **14**, 187 (1962).

- [6] M. J. Fisher and P. O. A. Davies, Correlation measurements in a non-frozen pattern of turbulence, *J. Fluid Mech.* **18**, 97 (1964).
- [7] J. A. B. Wills, On convection velocities in turbulent shear flows, *J. Fluid Mech.* **20**, 417 (1964).
- [8] J. C. D. Álamo and J. Jiménez, Estimation of turbulent convection velocities and corrections to Taylor's approximation, *J. Fluid Mech.* **640**, 5 (2009).
- [9] N. Renard and S. Deck, On the scale-dependent turbulent convection velocity in a spatially developing flat plate turbulent boundary layer at Reynolds number $Re_\theta = 13000$, *J. Fluid Mech.* **775**, 105 (2015).
- [10] R. H. Kraichnan, Kolmogorov's hypotheses and Eulerian turbulence theory, *Phys. Fluids* **7**, 1723 (1964).
- [11] H. Tennekes, Eulerian and Lagrangian time microscales in isotropic turbulence, *J. Fluid Mech.* **67**, 561 (1975).
- [12] G. W. He and J. B. Zhang, Elliptic model for space-time correlations in turbulent shear flows, *Phys. Rev. E* **73**, 055303 (2006).
- [13] X. Zhao and G. W. He, Space-time correlations of fluctuating velocities in turbulent shear flows, *Phys. Rev. E* **79**, 046316 (2009).
- [14] J. L. Lumley, Interpretation of time spectra measured in high-intensity shear flows, *Phys. Fluids* **8**, 1056 (1965).
- [15] M. Wilczek and Y. Narita, Wave-number-frequency spectrum for turbulence from a random sweeping hypothesis with mean flow, *Phys. Rev. E* **86**, 066308 (2012).
- [16] M. Wilczek, R. J. A. M. Stevens, and C. Meneveau, Spatio-temporal spectra in the logarithmic layer of wall turbulence: Large-eddy simulations and simple models, *J. Fluid Mech.* **769**, R1 (2015).
- [17] M. Wilczek, R. J. A. M. Stevens, and C. Meneveau, Height-dependence of spatio-temporal spectra of wall-bounded turbulence – LES results and model predictions, *J. Turbul.* **16**, 937 (2015).
- [18] A. Cenedese, G. P. Romano, and F. Defelice, Experimental testing of Taylor's hypothesis by L.D.A in highly turbulent flow, *Exp. Fluids* **11**, 351 (1991).
- [19] G. P. Romano, Analysis of two-point velocity measurements in near-wall flows, *Exp. Fluids* **20**, 68 (1995).
- [20] O. R. H. Buxton, R. de Kat, and B. Ganapathisubramani, The convection of large and intermediate scale fluctuations in a turbulent mixing layer, *Phys. Fluids* **25**, 125105 (2013).
- [21] R. de Kat and B. Ganapathisubramani, Frequency-wavenumber mapping in turbulent shear flows, *J. Fluid Mech.* **783**, 166 (2015).
- [22] B. J. McKeon and A. S. Sharma, A critical-layer framework for turbulent pipe flow, *J. Fluid Mech.* **658**, 336 (2010).
- [23] C. H. Geng, G. W. He, Y. S. Wang, C. X. Xu, A. Lozano-Durán, and J. M. Wallace, Taylor's hypothesis in turbulent channel flow considered using a transport equation analysis, *Phys. Fluids* **27**, 025111 (2015).
- [24] B. Q. Deng and C. X. Xu, Influence of active control on STG-based generation of streamwise vortices in near-wall turbulence, *J. Fluid Mech.* **710**, 234 (2012).
- [25] B. Q. Deng, W. X. Huang, and C. X. Xu, Origin of effectiveness degradation in active drag reduction control of turbulent channel flow at $Re_\tau = 1000$, *J. Turbul.* **17**, 758 (2016).
- [26] J. Kim, P. Moin, and R. D. Moser, Turbulence statistics in fully developed channel flow at low Reynolds number, *J. Fluid Mech.* **177**, 133 (1987).
- [27] R. D. Moser, J. Kim, and N. N. Mansour, Direct numerical simulation of turbulent channel flow up to $Re_\tau = 590$, *Phys. Fluids* **11**, 943 (1999).
- [28] J. C. D. Álamo and J. Jiménez, Spectra of the very large anisotropic scales in turbulent channels, *Phys. Fluids* **15**, L41 (2003).
- [29] H. Choi and P. Moin, On the space-time characteristics of wall-pressure fluctuations, *Phys. Fluids* **2**, 1450 (1990).
- [30] G. I. Park and P. Moin, Space-time characteristics of wall-pressure and wall shear-stress fluctuations in wall-modeled large eddy simulation, *Phys. Rev. Fluids* **1**, 024404 (2016).